Compensation of DC-link voltage oscillations in grid connected PV systems

Compensación de oscilaciones de voltaje en el enlace DC de sistemas fotovoltaicos conectados a la red

Carlos Andrés Ramos Paja[1], Giovanni Petrone[2], Andrés Julián Saavedra Montes[1]*

[1]Universidad Nacional de Colombia. Carrera 80 No 65-223. Medellín, Colombia.

[2]University of Salerno. Via Ponte Don Melillo 84084. Fisciano - Salerno - Italy.

(Recibido el 8 de marzo de 2010. Aceptado el 23 de mayo de 2012)

Abstract

This paper presents a compensation technique to mitigate the effect of DC-link voltage oscillations on PV systems. The main features of the technique are: the compensation is applied directly to the duty cycle, so it is simple to integrate with traditional maximum power point tracking systems; and the compensation calculation does not depend on the systems parameters, so its design is general. Explicit equations are provided for PV systems based on Boost, Buck and Buck-Boost dc/dc converters. Finally, the proposed approach is experimentally verified.

--------- *Keywords:* PV system, dc/dc converter, grid connection, maximum power point tracking

Resumen

Se presenta una técnica para compensar el efecto de las oscilaciones en el enlace DC en sistemas fotovoltaicos. Las principales características de la técnica son: la compensación se aplica directamente al ciclo de trabajo, por tanto es simple de integrar con sistemas tradicionales de maximización de potencia; y el cálculo de la compensación es independiente de los parámetros del sistema, por tanto el diseño es general. Se proveen ecuaciones explicitas para sistemas fotovoltaicos basados en convertidores dc/dc tipo Boost,

* Autor de correspondencia: teléfono: + 57 + 4 + 4255345, fax: +57 + 4 + 2341002, correo electrónico: caramosp@unal.edu.co (C. Ramos)

Buck y Buck-Boost. Finalmente, la solución se valida a través de resultados experimentales.

--------- *Palabras clave:* Sistemas fotovoltaicos, convertidores dc/dc, conexión a la red, seguimiento de punto de máxima potencia distribuida

Introduction

Photovoltaic (PV) applications are assuming a significant relevance in the production of worldwide energy, especially for the capability to produce energy in hostile contexts, like in emergent countries or in extreme environmental conditions. In such a cases small PV plants (lower than 10 kW), which are characterized by an extreme modularity and flexibility, are widely used for both stand-alone and grid-connected applications. The market of small PV systems is supported also by the increase of PV plants integrated in the urban context, installed with the aim of supplying energy locally. Such applications mainly include the Building Integrated PV (BIPV) systems, where the PV source contributes to make the buildings self-contained from the energetic point of view. Nonetheless in such a cases the probability of partial shading of the PV field might be not negligible and for this reason the PV field is decomposed in sub-modules, each one equipped with own power stage and Maximum Power Point Tracking (MPPT) controller [1]. As a consequence, the PV inverters dedicated to the small PV plants must be characterized by a large range for the input voltage in order to accept different configurations of the PV field. This capability is assured by adopting inverters based on a double stage architecture where the first stage, which usually is a dc/dc converter, can be used to adapt the PV array voltage in order to meet the requirements of the dc/ac second stage, which is used to supply an ac load or to inject the produced power into the grid. This configuration is effective also in terms of controllability because the first stage can be devoted to track the maximum power from the PV array, while the second stage is used to produce ac current with low Total Harmonic Distortion (THD).

The double-stage PV system presented in figure 1 is typically operated in two modes: (a) perturbing the duty cycle of the dc/dc converter to track the PV Maximum Power Point (MPP) [2], or (b) perturbing the reference of a control loop designed to regulate the PV voltage [3].

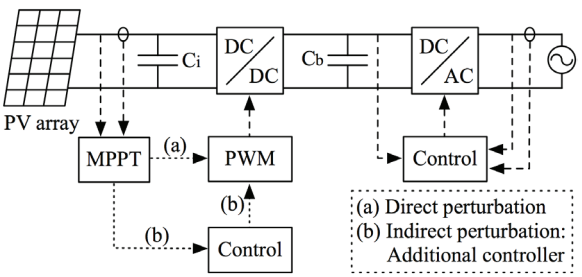

Figure 1 Double stage PV grid-connected system

The mode (a) is simpler from the implementation point of view because the MPPT is able to track the MPP for any uniform irradiance condition, but it is sensible to disturbances at the dc/dc converter output. Instead, mode (b) is able to reject load perturbations, but classically its design depends on the system parameters [3], so it is difficult to guarantee the designed behavior for all the operating range, and also it is not possible to provide a general controller for any application. Therefore, PV systems based on mode (a) are more general than those ones based on mode (b). Figure 2 presents the simulation of the PV system of figure 1 operating in mode (a) without any perturbation on the dc/dc converter output, namely the DC-link voltage V_b, considering also a Boost converter and a Kyocera KC120 PV panel [4]. In such a simulation the MPPT controller, which is based on a P&O algorithm [2], defines a three points behavior on the dc/dc converter duty cycle D, which denotes a correct MPPT operation and a stable profile [1, 2, 3].

Moreover, such stable D waveform is propagated to the PV voltage V_{PV} since

$$V_{PV} = V_b / M(D) \quad (1)$$

where M(D) = 1/(1-D) represents the Boost converter voltage conversion ratio in Continuous Conduction Mode (CCM) [5]. From (1) it is noted that stable D profiles generate stable V_{PV} profiles and consequently, if the D profile is settled on the basis of an MPPT algorithm [3], the power P_{PV}, generated by the PV module, will assume values near the maximum one. Such conditions are illustrated in figure 2, where D, V_{PV} and P_{PV} exhibit stable profiles, and the power extracted from the PV panel is 112 W, which corresponds to the KC120 maximum power at 35° temperature and 1000 W/m^2 irradiance. In the simulation the PV module is modeled by the non-linear equation given in (2), where the PV current I_{PV} and voltage V_{PV} are reported. I_{SC} is the PV short-circuit current and A and B are parameters [6] extracted from the datasheet.

$$I_{PV} = I_{SC} - A\left(1 - e^{B \cdot V_{PV}}\right) \quad (2)$$

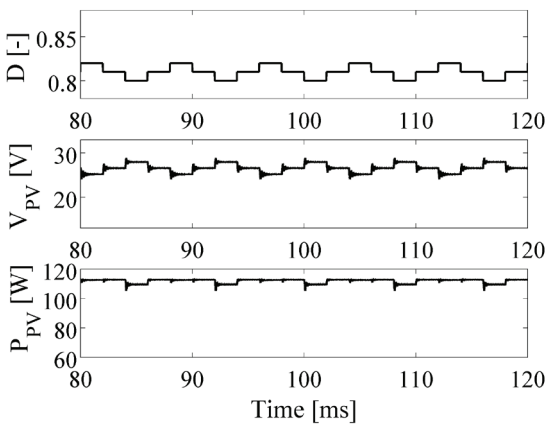

Figure 2 MPPT operation without V_b perturbation

In mono-phase applications, and in non-balanced three-phase ones, the double stage architecture presented in figure 1 exhibits voltage oscillations at the DC-link capacitor Cb, thus at the dc/dc converter output terminals. Such oscillations are caused by the difference between the sinusoidal power injected into the grid and the DC power extracted from the PV panel [3]. Moreover, such DC-link voltage V_b oscillations exhibit a sinusoidal profile with a frequency equal to the double of the grid frequency, and their amplitude is inversely to Cb [7].

Figure 3(a) presents a V_b perturbation caused by a small Cb capacitor, which generates a sinusoidal profile in the panel voltage V_{PV} if mode (a) is adopted. Such a V_{PV} profile confuses the MPPT algorithm [2, 3] leading to a sinusoidal power production far from the maximum power as depicted in figure 3(b), 112 W in this case.

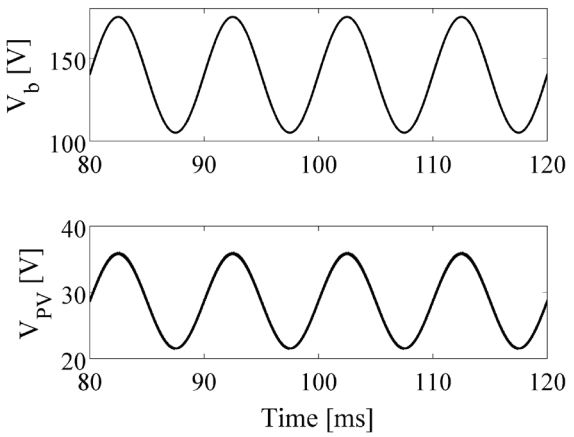

(a) Perturbation transmission to PV terminals

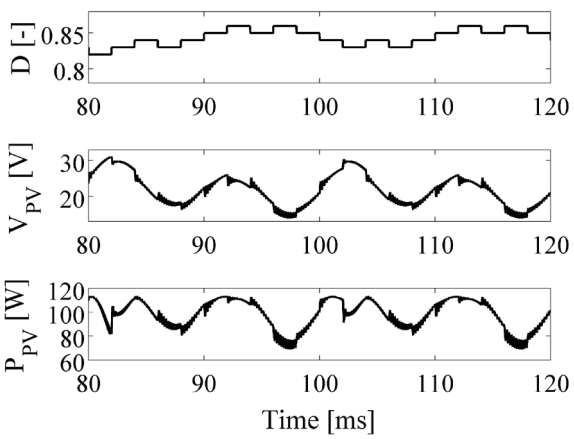

(b) MPPT operation

Figure 3 PV system operation with V_b perturbation

Contrasting P_{PV} in figure 2 and figure 3(b), it is evident that higher energy is produced with the MPPT operating without any V_b perturbation.

To address this problem, there are two classical approaches: adopt large electrolytic capacitors Cb to reduce V_b perturbations [7], or adopt mode (b), as in figure 1, to mitigate the DC-link voltage oscillations [3]. The use of electrolytic capacitors introduces reliability problems [7], and the use of classical controllers reduces the solution generality since their design depends on the system parameters and operating point. Therefore, this paper proposes a compensation technique, independent from the system parameters, to mitigate the DC-link voltage oscillations generated by using non-electrolytic capacitors with the dc/dc converter operating in CCM. In addition, the proposed solution can be easily integrated in classical mode (a) PV systems since it considers the compensation of the duty cycle instead of the PV voltage as in mode (b).

PV systems small-signal models

In the PV system presented in figure 1, the PV panel small-signal model corresponds to a differential resistance R_{PV} [2, 3] as in (3). Moreover, the closed loop inverter of figure 1 regulates the DC component of the DC-link voltage to ensure the required input voltage for its operation, and it is typically modeled by a voltage source acting as a load for the dc/dc converter [1, 3].

$$R_{PV} = V_{PV} / I_{PV} \tag{3}$$

In the following, the small-signal models of step-up, step-down, and step-up-down PV systems, without the MPPT controller, are analyzed considering dc/dc converters operating in CCM.

Boost based PV system

The electrical scheme of a step-up PV system based on a Boost converter is presented in figure 4, where u represents the Mosfet gate signal and i_L the inductor current.

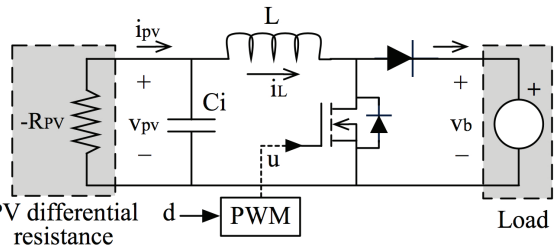

Figure 4 Boost based PV system: circuital scheme

The PV system is modeled in state space representation (4) considering the states vector **X**, inputs vector **U**, and output vector **Y** as in (5). Using the average modeling approximation [5], the state spaces matrices **Am**, **Bm**, **Cm**, and **Dm** are given in (6) and (7).

$$\dot{X} = Am\,X + Bm\,U, \qquad Y = Cm\,X + Dm\,U \tag{4}$$

$$\boldsymbol{X} = [i_L \quad v_{PV}]^T, \boldsymbol{U} = [d \quad v_b]^T, \boldsymbol{Y} = [v_{PV}] \tag{5}$$

$$\boldsymbol{Am} = \begin{bmatrix} 0 & 1/L \\ -1/C_i & -1/(R_{PV} \cdot C_i) \end{bmatrix}, \quad \boldsymbol{Bm} = \begin{bmatrix} v_b / L & -(1-d)/L \\ 0 & 0 \end{bmatrix} \tag{6}$$

$$\boldsymbol{Cm} = [0 \quad 1], \boldsymbol{Dm} = [0 \quad 0] \tag{7}$$

In order to analyze the small-signal behavior and stability, the previous model is linearized around an arbitrary desired operating point. This is done by considering the DC-link voltage equal to its DC component V_0 and the PV voltage equal to the desired one V_{PV0}. Moreover, the system equilibrium point is found from (4) by considering null the states derivatives, obtaining the following steady state duty cycle D_0 and inductor current I_L:

$$D_0 = 1 - V_{PV0} / V_0, \quad I_L = V_{PV0} / R_{PV} \tag{8}$$

The small-signal transfer functions between v_{PV} and d, $G_{PVd}(s)$, and v_b, $G_{PVb}(s)$, are:

$$G_{PVd}(s)=\frac{R_{PV}\cdot V_0}{L\cdot R_{PV}\cdot C_i\cdot s^2+L\cdot s+R_{PV}},\qquad G_{PVb}(s)=\frac{R_{PV}\cdot V_{PV0}/V_0}{L\cdot R_{PV}\cdot C_i\cdot s^2+L\cdot s+R_{PV}} \tag{9}$$

Buck based PV system

The electrical scheme of a step-down PV system based on a Buck converter is presented in figure 5 with the same considerations previously used for the Boost case.

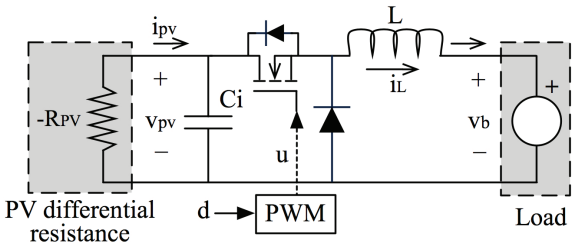

Figure 5 Buck based PV system: circuital scheme

The state space representation (4) of the PV system, considering **X**, **U**, and **Y** as in (5) is given by the matrices **Am**, **Bm**, **Cm**, and **Dm** reported in (10) and (11).

$$\boldsymbol{Am}=\begin{bmatrix}0 & d/L\\ -d/C_i & -1/(R_{PV}\cdot C_i)\end{bmatrix},\qquad \boldsymbol{Bm}=\begin{bmatrix}v_{PV}/L & -1/L\\ -i_L/C_i & 0\end{bmatrix} \tag{10}$$

$$\boldsymbol{Cm}=[0\quad 1],\quad \boldsymbol{Dm}=[0\quad 0] \tag{11}$$

The equilibrium point is defined by the steady state duty cycle and inductor current given in (12). Moreover, the transfer functions between v_{PV} and d, $G_{PVd}(s)$, and v_b, $G_{PVb}(s)$, are given in (13).

$$D_0=V_0/V_{PV0},\quad I_L=V_{PV0}/(R_{PV}\cdot D_0) \tag{12}$$

$$G_{PVd}(s)=\frac{(V_{PV0}^2/V_0)\cdot(V_{PV0}^2\cdot L\cdot s-V_0^2\cdot R_{PV})}{V_{PV0}^2\cdot L\cdot R_{PV}\cdot C_i\cdot s^2+V_{PV0}^2\cdot L\cdot s+V_0^2\cdot R_{PV}},\qquad G_{PVb}(s)=\frac{R_{PV}\cdot V_{PV0}\cdot V_0}{V_{PV0}^2\cdot L\cdot R_{PV}\cdot C_i\cdot s^2+V_{PV0}^2\cdot L\cdot s+V_0^2\cdot R_{PV}} \tag{13}$$

Buck-Boost based PV system

The electrical scheme of a step-up-down PV system based on a non-inverting Buck-Boost converter is presented in figure 6 with the same considerations adopted for the Boost case.

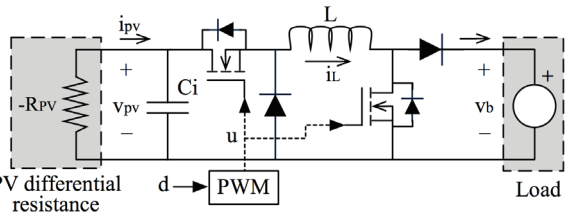

Figure 6 Buck-Boost based PV system: circuital scheme

The state space representation (4) of the PV system, considering **X**, **U**, and **Y** as in (5), is given by the matrices **Am**, **Bm**, **Cm**, and **Dm** reported in (14) and (15).

$$\boldsymbol{Am}=\begin{bmatrix}0 & d/L\\ -d/C_i & 1/(R_{PV}\cdot C_i)\end{bmatrix},\qquad \boldsymbol{Bm}=\begin{bmatrix}(v_{PV}+v_b)/L & -(1-d)/L\\ -i_L/C_i & 0\end{bmatrix} \tag{14}$$

$$\boldsymbol{Cm}=[0\quad 1],\quad \boldsymbol{Dm}=[0\quad 0] \tag{15}$$

The equilibrium point is defined by its duty cycle and inductor current given in (16), and the transfer functions between v_{PV} and d, $G_{PVd}(s)$, and v_b, $G_{PVb}(s)$, are given in (17).

$$D_0=V_0/(V_0+V_{PV0}),\quad I_L=V_{PV0}/(R_{PV}\cdot D_0) \tag{16}$$

$$G_{PVd}(s)=\frac{V_{PV0}\cdot\left(\lambda\cdot V_0+3\cdot\psi\cdot V_0+3\cdot\psi\cdot V_{PV0}^2+\delta\cdot V_{PV0}\right)\cdot s-\left(\phi\cdot V_0^2-2\cdot\phi\cdot V_0\cdot V_{PV0}-\phi\cdot V_{PV0}^2\right)}{V_0\cdot\left(\alpha+\beta_i+\varphi\right)\cdot s^2+V_0\cdot\left(\lambda+2\cdot\psi+\delta\right)\cdot s+V_0\cdot\phi},$$

$$G_{PVb}(s)=\frac{R_{PV}\cdot V_{PV0}\cdot V_0}{\left(\alpha+\beta_i+\varphi\right)\cdot s^2+\left(\lambda+2\cdot\psi+\delta\right)\cdot s+\phi}, \quad (17)$$

$$\alpha=V_0^2\cdot L\cdot R_{PV}\cdot C_i,\beta=2\cdot V_0\cdot L\cdot R_{PV}\cdot V_{PV0}\cdot C_i,\varphi=L\cdot R_{PV}\cdot V_{PV0}^2\cdot C_i$$

$$\lambda=V_0^2\cdot L,\psi=V_0\cdot L\cdot V_{PV0},\delta=L\cdot V_{PV0}^2,\phi=V_0^2\cdot R_{PV}$$

DC-link voltage oscillations compensator

From the basic relation between the input and output ports of the dc/dc converter given in (1), it is noted that any oscillation at V_b is transmitted to V_{PV} if the converter input/output voltages ratio M(D) is constant. Moreover, M(D) is a non-linear function that depends exclusively on the duty cycle D if parasitic losses are not considered. Therefore, constant D generates constant M(D).

Since the MPPT controller provides the steady state duty cycle D_0 aimed at maximizing the PV power production, as in mode (a) of figure 1, an additional component ΔD must be added to the duty cycle to compensate the voltage oscillations ΔV_b at the DC-link. Such compensation architecture is presented in figure 7.

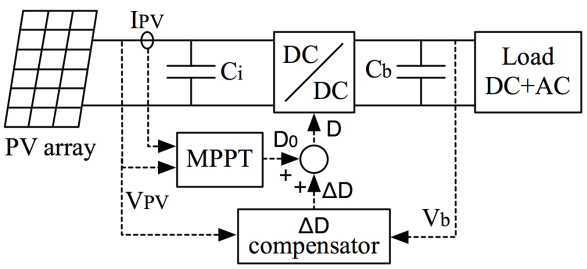

Figure 7 Compensator architecture

From the analyses of Boost, Buck and Buck-Boost PV systems previously presented, assuming the states derivatives equal to zero to obtain the steady state relations for any V_{PV} and V_b conditions, the duty cycle for the Boost, Buck and Buck-Boost converters are:

$$D=\begin{cases}1-V_{PV}/V_b\text{, for Boost}\\ V_b/V_{PV}\text{, for Buck}\\ V_b/(V_b+V_{PV})\text{, for Buck - Boost}\end{cases} \quad (18)$$

In addition, the duty cycle of the converters to obtain the desired V_{PV0} voltage at the PV panel terminals from the DC component V_0 of the DC-link voltage, are:

$$D_0=\begin{cases}1-V_{PV0}/V_0\text{, for Boost}\\ V_0/V_{PV0}\text{, for Buck}\\ V_0/(V_0+V_{PV0})\text{, for Buck - Boost}\end{cases} \quad (19)$$

Since the DC-link voltage exhibits both V_0 and ΔV_b components (20), the duty cycle must to exhibit the additional ΔD component given in (21) to mitigate the DC-link oscillations. Such a duty cycle compensation for Boost, Buck and Buck-Boost converters is given in (22).

$$V_b=V_0+\Delta V_b \quad (20)$$

$$\Delta D=D-D_0 \quad (21)$$

$$\Delta D=\begin{cases}\left(V_{PV}\cdot\Delta V_b\right)/\left(V_b\cdot V_0\right)\text{, for Boost}\\ \Delta V_b/V_{PV}\text{, for Buck}\\ \left(V_{PV}\cdot\Delta V_b\right)/\left[\left(V_b+V_{PV}\right)\cdot\left(V_0+V_{PV}\right)\right]\text{, for Buck - Boost}\end{cases} \quad (22)$$

Stability analysis

To provide a stability analysis, the small-signal models of the PV systems, considering the duty cycle compensation, are obtained. Moreover, the oscillation component ΔV_b of the DC-link must be obtained by means of an arbitrary order band-pass filter. The duty cycle compensation Δd is calculated by considering a correct operation of the compensation technique, so $v_{PV} = V_{PV0}$, and a small-signal perturbation Δv_b, therefore $V_b \approx V_0$. The band-pass filter used to obtain Δv_b is:

$$\Delta v_b(s) = G_{nf}(s) \cdot v_b(s) \tag{23}$$

From such considerations, and replacing (23) in (22), the small-signal compensations Δd are:

$$\Delta d(s) = K_{sa} \cdot G_{nf}(s) \cdot v_b(s), \quad \begin{cases} K_{sa} = V_{PV0}/V_0^2 \text{ for Boost} \\ K_{sa} = 1/V_{PV0} \text{ for Buck} \\ K_{sa} = V_{PV0}/(V_{PV0} + V_0)^2 \text{ for Buck - Boost} \end{cases} \tag{24}$$

Figure 8 presents the block diagram of the small-signal model, where the compensated transfer functions from d_0 and v_b to the output v_{PV}, $T_{PVd}(s)$ and $T_{PVb}(s)$ respectively, are given in (25).

$$\begin{aligned} T_{PVd}(s) &= v_{PV}(s)/d_0(s) = G_{PVd}(s), \\ T_{PVb}(s) &= v_{PV}(s)/v_b(s) = G_{PVb}(s) + G_{PVd}(s) \cdot G_{nf}(s) \cdot K_{sa} \end{aligned} \tag{25}$$

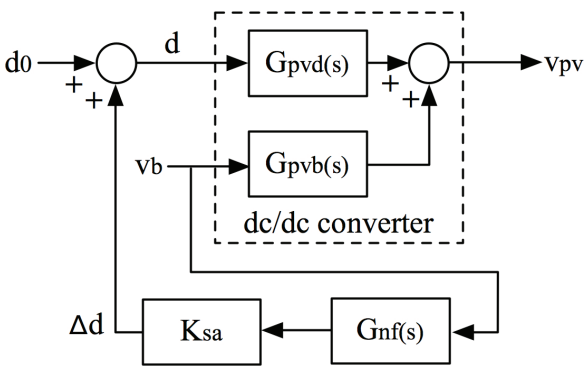

Figure 8 Small-signal block diagram

Generalizing the transfer functions of the dc/dc converter and filter as in (26), the compensated transfer functions (25) are expanded as in (27). Therefore, the poles of the compensated transfer functions correspond to the open loop poles of the dc/dc converter and filter, which are always stable [5], and the compensated system will be stable regardless the converter topology. Such a condition permits to adopt the proposed technique to any PV system based on a dc/dc converter.

$$G_{PVd}(s) = P_{PVd}(s)/Q_{PVd}(s), \quad G_{PVb}(s) = P_{PVb}(s)/Q_{PVb}(s), \quad G_{nf}(s) = P_{nf}(s)/Q_{nf}(s) \tag{26}$$

$$\begin{aligned} T_{PVd}(s) &= P_{PVd}(s)/Q_{PVd}(s), \\ T_{PVb}(s) &= \frac{P_{PVb}(s) \cdot Q_{PVd}(s) \cdot Q_{nf}(s) + P_{PVd}(s) \cdot P_{nf}(s) \cdot Q_{PVb}(s) \cdot K_{sa}}{Q_{PVb}(s) \cdot Q_{PVd}(s) \cdot Q_{nf}(s)} \end{aligned} \tag{27}$$

To illustrate the system stability, a second order filter is adopted (28), where B represents the -3 dB bandwidth of the band-pass filter and ω_0 the center frequency in rad/s.

$$G_{nf}(s) = \frac{k_f \cdot B \cdot s}{s^2 + B \cdot s + \omega_0^2} \tag{28}$$

The poles of $G_{nf}(s)$, $T_{PVb}(s)$ and $T_{PVd}(s)$ for the Boost, Buck and Buck-Boost converters are

given in (29) and (30), where it is confirmed that both $T_{PVb}(s)$ and $T_{PVd}(s)$ are always stable since the real parts of s_{nf}, s_{PVd} and s_{PVb} are negative for positive values of B, L, C_i, V_{PV0}, V_0, and R_{PV}. R_{PV} is always positive because $I_{PV} > 0$ (3). Therefore, the compensated system is always stable.

$$s_{nf} = \left(-B \pm \sqrt{B^2 - 4 \cdot \omega_0^2}\right)/2 \tag{29}$$

$$s_{PVd} = s_{PVb} = \begin{cases} \dfrac{-L \pm \sqrt{L^2 - 4 \cdot L \cdot C_i \cdot R_{PV}^2}}{2 \cdot L \cdot C_i \cdot R_{PV}}, \text{for Boost} \\ \dfrac{-L \cdot V_{PV0} \pm \sqrt{L^2 \cdot V_{PV0}^2 - 4 \cdot L \cdot C_i \cdot R_{PV}^2 \cdot V_0^2}}{2 \cdot L \cdot C_i \cdot R_{PV} \cdot V_{PV0}}, \text{for Buck} \\ \dfrac{-L \cdot (V_{PV0} + V_0) \pm \sqrt{L^2 \cdot (V_{PV0} + V_0)^2 - 4 \cdot L \cdot C_i \cdot R_{PV}^2 \cdot V_0^2}}{2 \cdot L \cdot C_i \cdot R_{PV} \cdot (V_{PV0} + V_0)}, \text{for Buck - Boost} \end{cases} \tag{30}$$

Band-pass filter design

The center frequency ω0 of the band-pass filter must be set at the double of the grid frequency, 100 Hz in Europe and 120 Hz in America. The bandwidth B must be set in agreement with the grid frequency oscillations, but in general a larger B provides a better mitigation of ΔV_b oscillations since more frequencies are filtered. The effect of B on both the band-pass filter and the compensated system frequency responses is illustrated in figure 9, it considering a Boost converter and the following parameters: V_{PV0} = 28.7 V, V_0 = 140 V, I_{PV} at V_{PV0} = 3.7 A, I_{SC} = 5 A, C_i = 22 μF, L = 47 μH, $\omega_0 = 2\times n(\pi)\times 100$ rad/s, k_f = 1, and a F_{SW} = 50 kHz switching frequency.

Figure 9 shows that for any value of B, the compensated PV system accurately rejects the frequency component selected by ω_0, but a larger B provides robustness against grid frequency variation. Moreover, equation (27) and figure 9 also show that additional band-pass filters can be introduced to reject multiple components, i.e. grid noise injected by electromechanical machines.

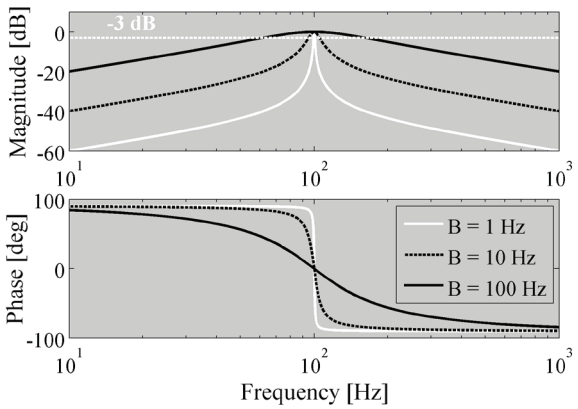

(a) Band-pass filter

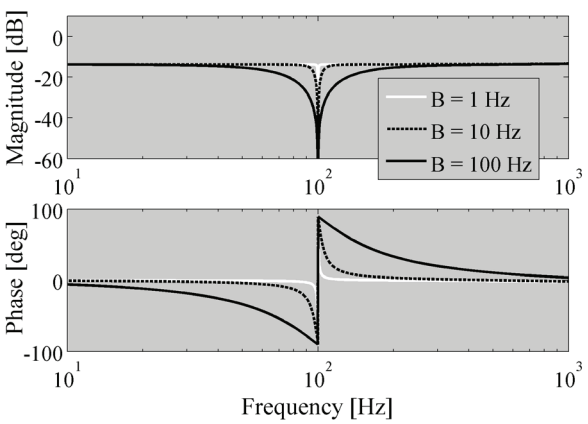

(b) Compensated PV system

Figure 9 Effect of the Band-pass filter bandwidth

Finally, figure 10 presents the frequency responses of the compensated PV systems based on Boost, Buck, and Buck-Boost converters. Such diagrams were obtained by simulating the non-linear circuits and compensators in the power electronics simulator PSIM, and by means of the small-signal models calculated in (27). It is noted the accurate representation of the non-linear circuits provided by the models, which confirms the validity of the previous analyses.

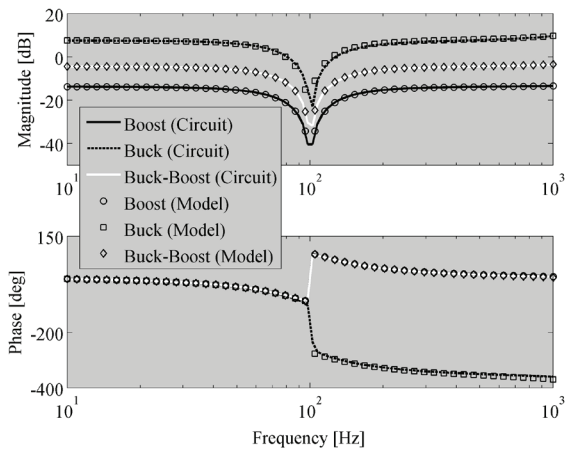

Figure 10 PV systems frequency responses: circuit and model comparison

Simulation results

The effectiveness of the compensation technique was tested using the parameters previously defined for the Boost case with B = 2×n(π)×100 rad/s, V_0 = 12 V for the Buck case and V_0 = 48 V for the Buck-Boost case. Such conditions guarantee the consistency of the simulation results. Moreover, a 100 Hz oscillation on the DC-link voltage, with a peak-to-peak amplitude of 50 % of the DC voltage, was considered to test the compensation systems.

Figure 11(a) shows the simulation of the Boost-based PV system where, as predicted in figure 10, the 100 Hz ΔV_b perturbation is successfully mitigated. The figure also permits to contrast the system behavior with and without compensation. Figure 11(b) confirms that the compensated system of figure 7 is able to operate with a traditional MPPT controller in the same way as in classical mode (a), rejecting the effect of oscillations at the DC-link. In such a simulation the same MPPT controller used in figure 2 was considered, obtaining the same power but in presence of a 50 % ΔV_b perturbation. Such a condition makes possible to adopt non-electrolytic capacitors.

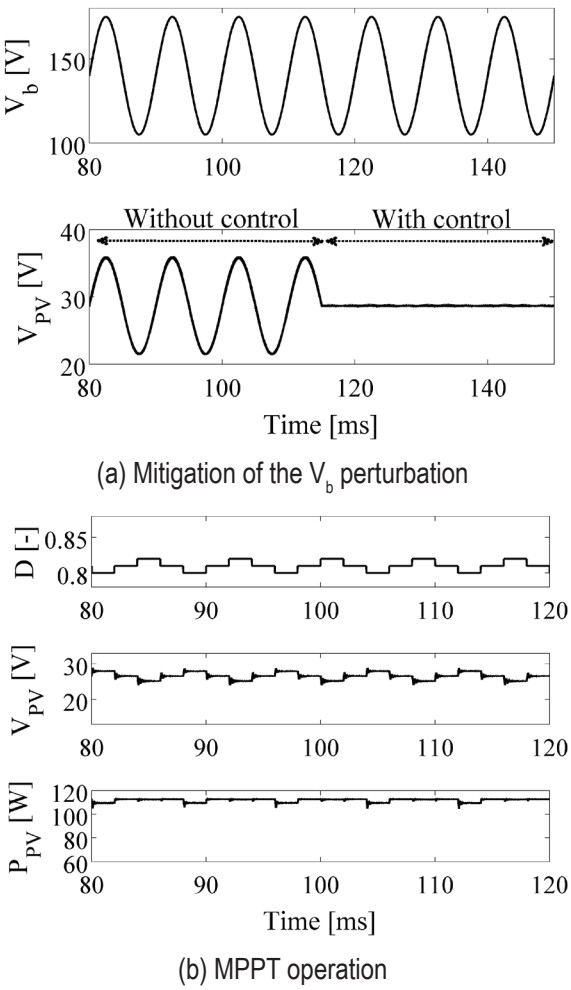

Figure 11 Boost based PV system control

Similarly, figure 12 shows the simulation of the PV systems based on Buck and Buck-Boost converters. As predicted in figure 10, the 100 Hz ΔV_b perturbation is successfully mitigated in both cases by means of the calculated ΔD compensators. It is noted a higher ripple in the Buck case since the same capacitor was used for all the converters to provide a fair comparison.

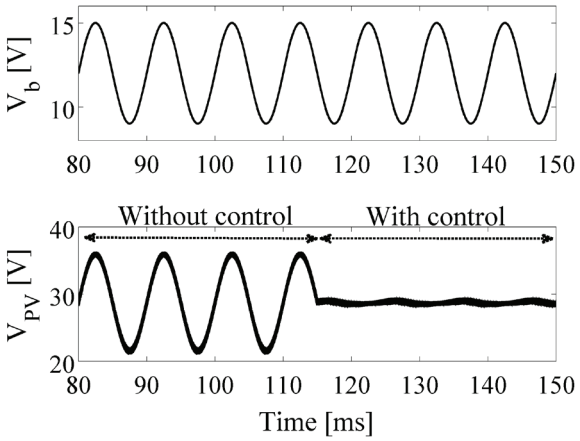

(a) Buck based system

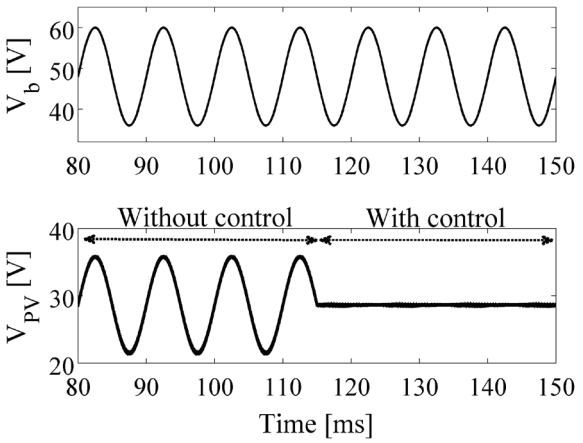

(b) Buck-Boost based system

Figure 12 Control of Buck and Buck-Boost based PV systems: mitigation of the V_b perturbation

Experimental results

The behavior predicted by the analytical and simulation results was experimentally verified. The correctness of the approach was illustrated by means of a *proof of concept* PV system based on a Boost converter, which requires a low-side circuitry for driving the active devices, simplifying the practical implementation in comparison to the Buck and Buck-Boost cases. The applicability of the proposed duty cycle compensations to the Buck and Buck-Boost cases has been demonstrated by means of the simulation results. Figure 13(a) shows the block diagram of the experimental system using a Kyocera KC120 PV panel and an electronic load that imposes a 50 % ΔV_b perturbation at 100 Hz. The duty cycle compensation is calculated in a Xilinx Spartan3 XC3S1500 FPGA mounted in an Opal Kelly XEM 3010 board [8], and the PV and V_b voltages are acquired by means of an Analog to Digital Converter (ADC). In addition, the band-pass filter, the PWM, and the steady state duty cycle D_0 are programmed inside the FGPA. Finally, the laboratory setup is presented in figure 13(b).

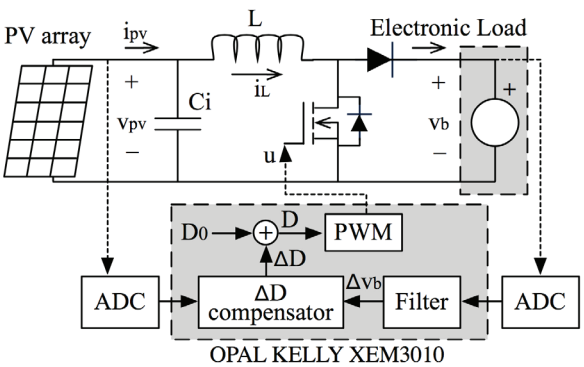

(a) Block diagram

(b) Laboratory setup

Figure 13 Experimental system

Figure 14(a) shows the PV system operation without the duty cycle compensation exhibiting the propagation of the 100 Hz oscillations from the DC-link to the PV panel terminals. Instead, figure 14(b) shows the PV system operation using the duty cycle compensation, where the V_b

perturbations were attenuated to less than 1 V, which is acceptable since the DC-link oscillations exhibit additional low frequency components generated by the electronic load current absorption.

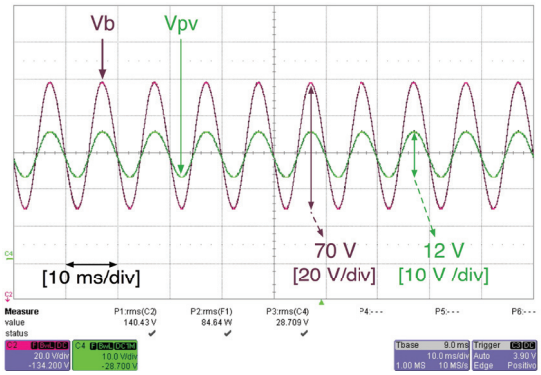

(a) Without duty cycle compensation

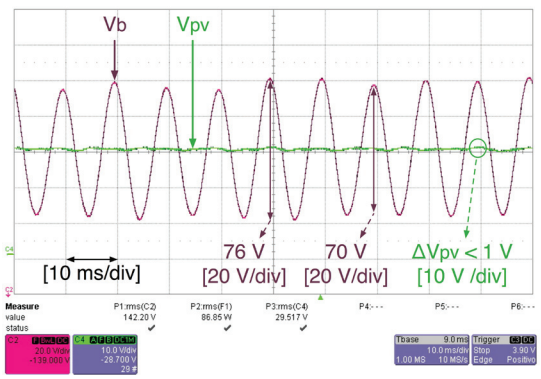

(b) With duty cycle compensation

Figure 14 Experimental results

Conclusions

A duty cycle compensation technique to mitigate the effect of DC-link voltage oscillations on PV systems has been presented. Explicit design equations have been provided for systems based on Boost, Buck and Buck-Boost dc/dc converters operating in CCM. Such equations do not depend on the systems parameters, therefore they are applicable to any system exhibiting the same circuitry. If discontinuous conduction mode [5] is required, different equations must be derived. Small-signal models of the PV systems have been calculated, demonstrating the stability of the compensated systems. In addition, the compensators have been validated by means of simulation results, and satisfactory experimental results have confirmed the correctness of the technique. Finally, the duty cycle compensation can be improved by considering parasitic elements, additional dc/dc converter topologies, and the operation in discontinuous conduction mode.

Acknowledgments

This work was supported by the GAUNAL group of the Universidad Nacional de Colombia under the project SMART-ALEN, the scholarship 095-2005 from COLCIENCIAS, and by the FARB2011 of the University of Salerno.

References

1. N. Femia, G. Lisi, G. Petrone, G. Spagnuolo, M. Vitelli, "Distributed Maximum Power Point Tracking of Photovoltaic Arrays: Novel Approach and System Analysis." *IEEE Transactions on Industrial Electronics.* Vol. 55. 2008. pp. 2610-2621.

2. N. Femia, G. Petrone, G. Spagnuolo, M. Vitelli. "Optimization of perturb and observe maximum power point tracking method." *IEEE Transactions on Power Electronics*. Vol. 20. 2005. pp. 963-973.

3. N. Femia, G. Petrone, G. Spagnuolo, M. Vitelli. "A technique for improving P&O MPPT performances of double-stage grid-connected photovoltaic systems." *IEEE Transactions on Industrial Electronics*. Vol. 56. 2009. pp. 4473-4482.

4. Kyocera. "Kyocera KC-120 PV panel datasheet". On line: http://www.kyocerasolar.eu/index/products/download/German.-cps-61757-files-87160-File.cpsdownload.tmp/DB-E-KC120-1.pdf. Accessed on: May 8. 2012.

5. R. Erickson, D. Maksimovic. *Fundamentals of Power Electronics.* 2nd ed. Ed. Springer. Norwell, United States of America. 2001. pp. 13-125.

6. G. Petrone, C. Ramos. "Modeling of photovoltaic fields in mismatched conditions for energy yield evaluations." *Electric Power Systems Research*. Vol. 81. 2011. pp. 1003-1013.

7. G. Petrone, G. Spagnuolo, R. Teodorescu, M. Veerachary, M. Vitelli. "Reliability Issues in Photovoltaic Power Processing Systems." *IEEE Transactions on Industrial Electronics.* Vol. 55. 2008. pp. 2569-2580.

8. Xilinx. "Opal Kelly XEM 3010 board". On line: http://www.opalkelly.com/products/xem3010. Accessed on: May 8. 2012.